Comparison of Thermally Driven Circulations from a Depth-Coordinate Model and an Isopycnal-Layer Model. Part I: Scaling-Law Sensitivity to Vertical Diffusivity

YOUNG-GYU PARK AND KIRK BRYAN

Program in Atmospheric and Oceanic Sciences, Princeton University, Princeton, New Jersey

ABSTRACT

Two different types of numerical ocean circulation models are used in a classical idealized problem, the thermally induced circulation in an ocean basin bounded by two meridians to the east and west and by the equator and a line of constant latitude. A simple scaling theory exists for predicting poleward heat transport and the strength of meridional overturning as a function of vertical diffusivity and other external factors. However, previous studies have indicated conflicting results, and other scaling laws have been proposed. Experiments with two widely used types of numerical models, one based on depth coordinates and the other based on isopycnal layers, provide insight into the discrepancies of previous studies. In the numerical experiments vertical diffusivity is varied over a range of 200. The source of the difficulty in previous studies is in part traced to applying a fixed restoring coefficient at the upper boundary and considering the buoyancy forcing at the surface fixed irrespective of vertical diffusivity κ. Globally or zonally averaged results show a robust agreement between the two models and support the simple scaling law in a flat-bottom basin and a bowl-shaped basin, as long as the meridional circulation is estimated along isopycnal surfaces and in situ rather than externally imposed restoring density differences are used to estimate the geostrophic-scale velocity. Over the thermocline the vertical mean of the zonally averaged zonal baroclinic pressure gradient has constant ratio to the vertical mean of the zonally averaged meridional baroclinic pressure gradient, consistent with the scaling assumptions for a diffusive thermocline.

1. Introduction

Direct observations of the ocean are now, and in the foreseeable future, insufficient to provide an understanding of the ocean circulation and the role of the World Ocean in climate. As in atmospheric science, oceanographers will become increasingly dependent on models to analyze oceanographic data and provide insight on large-scale air–sea interaction. One way to test ocean models is by directly comparing simulations driven by known surface boundary conditions and initial conditions based on observed hydrographic data.

A recent example of this type of test is the "DYNAMO Project" (DYNAMO Group 1997), a cooperative effort carried out by several European laboratories. Three numerical models, each based on a very different finite difference representation of the vertical coordinate systems are compared. The initial value problem, which

is solved for the three cases, produces circulation patterns for the North Atlantic that are quite distinct. The comparison reveals that the three models give somewhat similar results in low-latitude areas that are well stratified, but there are significant differences in the subpolar areas of the North Atlantic where the stratification is weaker and active water mass formation is taking place. While the results obtained in this type of study are very important for testing parameters and analyzing observational data, there are difficulties in obtaining a detailed understanding of simulations in such a complex geometry with realistic forcing.

In the present study the goal has been to analyze in detail a much simpler, idealized problem, using two of the three types of models compared in the DYNAMO Project. Since the calculations are much easier to carry out, it is possible to find equilibrium solutions over a wide range of vertical diffusivity, the most important parameter for determining the intensity of the thermohaline circulation. The idealized geometry in our numerical experiments does not allow a comparison with observations, but previous studies based on simplified analytical models and numerical solutions provide a good basis for understanding the solutions and the effects of different numerical representations. The aim is to provide a simplified basis for obtaining insights into more complex models.

---

* Current affiliation: Center for Ocean–Land–Atmosphere Studies, Calverton, Maryland.

Corresponding author address: Young-Gyu Park, Center for Ocean–Land–Atmosphere Studies, 4041 Powder Mill Rd., Suite 302 Calverton, MD 20705-3106.
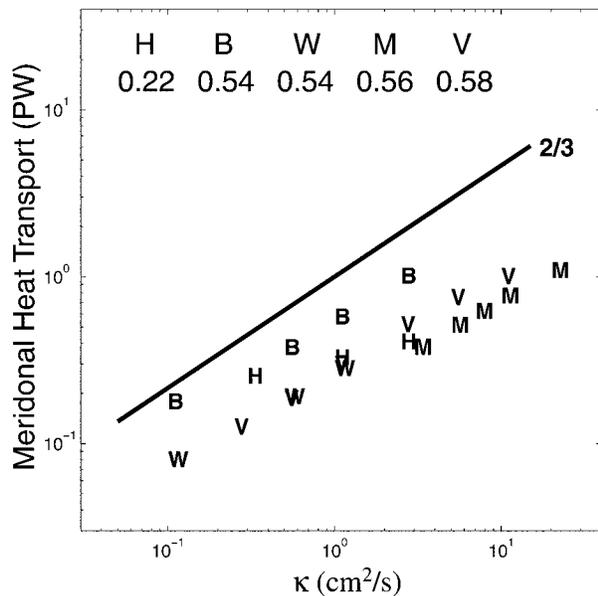E-mail: ypark@cola.iges.org

FIG. 1. Results from earlier studies. **B** is for Bryan (1987), **V** is for Colin de Verdière (1988), **W** is for Winton (1996), **H** is for Hu (1996), and **M** is for Marotzke (1997). Single hemispheric sector basins with flat-bottom geometry are used in all cases. **B**, **W**, and **M** are from depth coordinate models based on primitive equations, **V** is from a depth coordinate model based on planetary geostrophic equation, and **H** is from an isopycnal layer model. In **M**, κ is nonzero along eastern and western boundaries. In other cases κ is uniform throughout the domain. Surface wind stress is considered in **B** and **H**. Numbers represents the power dependence of the meridional heat transport on κ for each case.

Based on earlier studies by Robinson and Stommel (1959) and Lineikin (1955), Bryan and Cox (1967) developed a simple scaling law for the thermohaline circulation based on geostrophic balance and an advective–diffusive heat balance. Details of this scaling are given in section 2. Later studies of numerical models showed general agreement with some parts of this scaling, but the results for other aspects are ambiguous. The meridional heat transport obtained by various authors are shown in Fig. 1. Since the absolute values of heat transport depend on the exact geometry employed in the different experiments, the significant feature in Fig. 1 is the power-law relationship between the vertical diffusivity κ and meridional heat transport. The actual power laws found by the different authors given at the top of the figure range from 0.22 obtained by the isopycnal model of Hu (1996) to 0.58 found in the experiments of Colin de Verdière (1988). The scaling law of Bryan and Cox (1967) indicates a ⅔ law, the solid line in the figure.

Some of the differences may easily be accounted for by the different configuration of the sets of experiments carried out by different authors. In some cases the effects of wind are included and in others not. Bryan (1987) and Winton (1996) favored a ⅔ law, while Colin de Verdière (1988) and Marotzke (1997) preferred a ½

law for the dependence of heat transport as a function of κ. By estimating the mean zonal density gradient, Marotzke (1997) developed a new theory to explain his result. Certainly all the results with the exception of Hu's (1996) range between 0.54 and 0.58, so both possibilities appeared to be equally plausible.

In other respects previous experiments do not correspond to the Bryan and Cox (1967) scaling. Bryan (1987) found that the strength of the meridional overturning of his thermohaline circulation Ψ has about half the sensitivity to vertical diffusivity predicted. Colin de Verdière (1988) considered kinetic energy as a measure of the strength of the overturning circulation and concluded that his result does not obey the scaling law. Huang and Chou (1994) argue that the discrepancy in Bryan's (1987) results is because his calculations were not fully in thermal equilibrium. However, even after reaching equilibrium states their results yield a ½ power law, consistent with the conclusion of Colin de Verdière (1988). Winton (1996) interprets this discrepancy in Bryan's (1987) results in another way. He suggests that the maximum transport streamfunction at the northern sinking region used by Bryan (1987) is not a good measure. He obtains a reasonable agreement between the scaling law and the strength of the overturning estimated at some distance away from the sinking region.

Recently, Marotzke (1997) found a good agreement between the ⅔ law and Ψ both at high latitudes and midlatitudes in his experiment in which the vertical diffusivity was confined to bands along the meridional boundaries. It is interesting to note that the earlier studies mentioned above could not obtain such a good agreement at high latitudes even though similar numerical models were used. It remains unclear if the result of Marotzke (1997) may be accounted for by enhanced mixing along the meridional boundaries. Zhang et al. (1999) also show that Ψ of their numerical experiments using the eddy mixing parameterization of Gent and McWilliams (1990) follows the ⅔ law. They suggest that the good agreement is due to the inclusion of an eddy mixing scheme that eliminates false diapycnal mixing due to horizontal mixing, especially when the slope of the isopycnals is large.

These ambiguities in the analysis of highly idealized models of the thermohaline circulation show the extreme difficulty of interpreting numerical experiments. Thus the aim of this study is an attempt to establish a reference by a series of systematic numerical experiments in which a model based on isopycnal coordinates designed by Hallberg (Hallberg and Rhines 1996) is compared with a version of the GFDL MOM model (Pacanowski 1995) based on depth coordinates. Hereafter the Hallberg model will be referred to as the layered model and the MOM model as the *z* model. The main focus is the power-law dependence between κ, the vertical diffusivity, and quantities of interest to climate such as poleward heat and mass transports and the ther-

mocline depth. In other words, we wish to answer two questions:

1) Do numerical models based on radically different vertical coordinate systems give the same results for the thermally driven circulation?
2) What is the scaling law that best relates the vertical diffusivity to climatically important quantities, like poleward heat transport?

The experiments are carried out in a single hemispheric basin with mirror symmetry across the equator. The basin is bounded in the poleward direction by a wall at 60° latitude, and by two meridians 60 degrees of longitude apart. The horizontal resolution is 2° in both models. In the z model, there are 20 levels vertically with thickness varying from 25 m over the upper 200 m to 603 m at the bottom. The thermal diffusivity is varied from 0.05×10^{-4} to 10.0×10^{-4} m² s⁻¹. This is a factor of 200, a much larger range than used in previous studies. We have used this large range in order to get a more accurate estimate of the power dependence of the solution on the thermal diffusivity. Since recent measurements by Ledwell et al. (1993) suggest that vertical diffusion in the main thermocline could be much less than the canonical value suggested by Munk (1966), it was considered particularly important to extend the calculations to very low thermal diffusivity. Two sets of experiments are carried out. In one set the basin has a uniform depth of 4000 m. As emphasized by Winton (1997), continental shelves can change ocean circulation significantly. Therefore a second set of experiments was carried out in which a narrow shelf is included on the poleward and meridional boundaries.

As pointed out by Veronis (1975) horizontal diffusivity in a z model can cause diapycnal diffusion, the so-called Veronis effect, which is absent in a model based on isopycnal coordinates. This effect may cause diapycnal mixing to be dominated by numerical rather than explicit mixing when κ is small. To run the z model with very small κ without horizontal diffusivity and to compare the types of models more directly, the flux-corrected method of Boris and Book (1973) is used.

The paper is organized as follows: the scaling law of Bryan and Cox (1967) is reviewed in section 2, the models and configuration of the experiments are given in section 3, and a comparison of the scaling law and the experimental results are given in section 4, including a discussion of earlier studies. Finally, conclusions and a summary of results are in section 5. This paper concentrates on globally or zonally averaged properties of the solutions, which are found to agree quite well for the two types of numerical models tested. Part II will analyze the solutions in a more general way and relate the numerical solutions to previous analytic studies of the thermohaline circulation.

2. The scaling law

Pioneering work on scaling the thermohaline circulation was carried out by Lineikin (1955), and Robinson and Stommel (1959). [Reviews can be found in Welander (1986).] Bryan and Cox (1967) made the first attempt to use these ideas to analyze the results of a numerical model of the ocean circulation. Let us consider a simple two-dimensional overturning circulation in a basin of planetary scale driven by a poleward density gradient imposed at the upper surface. As a response to the imposed density gradient we expect sinking near the poleward boundary, which is compensated by a general poleward flow near the surface. If vertical diffusivity is present, we expect a low-density boundary layer corresponding to the main thermocline of the ocean to form near the surface of the model "ocean." Robinson and Stommel (1959) show how an advective–diffusive balance determines the depth of the thermocline. The basic idea behind the thermocline scaling without wind is that a change in the vertical diffusion only changes the vertical scale of the thermocline and that the horizontal patterns are self-similar.

Within the thermocline of such a model, geostrophic thermal wind balance yields an estimate of the horizontal velocity scale, U

$$U \equiv \frac{g\alpha\Delta T\delta_T}{fL}. \qquad (1)$$

Here g is the acceleration of gravity, α is the thermal expansion coefficient, and $g\alpha\Delta T$ is a measure of the total poleward buoyancy difference imposed at the upper boundary; L and δ_T are measures of the horizontal scale of the basin and depth of the thermocline, respectively, and f is the rotation. Since the intensity of the geostrophically balanced thermocline circulation depends on zonal rather than meridional density gradients, the scaling depends on the implicit assumption that there is a linear relation between the scale velocities appropriate for the zonal and meridional directions. This assumption is verified a posteriori from the experiments. The result is shown in section 4.

The meridional flow in the upper layers of the model needed to compensate sinking at the poleward boundary must be compensated by interior upwelling. Thus continuity provides a measure of the scale of the vertical velocity in the interior, W

$$W \equiv \frac{U\delta_T}{L}. \qquad (2)$$

The balance between the upwelling of cold water at the base of the thermocline and thermal diffusion (Munk 1966)

$$wT_z \approx \kappa T_{zz}$$

yields another measure of the vertical scale velocity given in Eq. (3)

$$W \equiv \frac{\kappa}{\delta_T}. \qquad (3)$$

Combining Eqs. (1)–(3) we get expressions for the thermocline depth and the horizontal velocity

$$\delta_T = \left(\frac{\kappa L^2 f}{g\alpha\Delta T}\right)^{1/3}, \qquad (4)$$

$$U = \left(\frac{\kappa(g\alpha\Delta T)^2}{Lf^2}\right)^{1/3}. \qquad (5)$$

A measure of the intensity of the thermohaline circulation (or meridional mass transport) Ψ is

$$\Psi \equiv U\delta_T L = \left(\frac{\kappa^2 L^4 g\alpha\Delta T}{f}\right)^{1/3}. \qquad (6)$$

Meridional poleward heat transport H is thus

$$H \equiv \rho_o C_p \Delta T \Psi = \rho_o C_p \left(\frac{L^4 g\alpha\kappa^2\Delta T^4}{f}\right)^{1/3}. \qquad (7)$$

Closed analytic solutions are not available as a basis for this scaling, so our approach is empirical. Comparison between the predictions of the scaling law and the results of numerical experiments provides a test of the fundamental assumptions.

The classical thermocline theory of Robinson and Stommel (1959) defined the vertical scale velocity from the linear vorticity equation in a β plane instead of from the continuity equation as in Eq. (2). Therefore, the scales for velocity and thermocline from the thermocline theory show explicit dependence on β, while the scaling law described in this section does not. If the β effect is defined as f/L, Robinson and Stommel's final result is identical for a basin with dimensions comparable to the radius of the earth. [They did not derive a scale for meridional heat transport, but their theory yields the same result if we use the definition in Eq. (7).]

3. Models

There are some important details that are different in the z model and the layered model used in the experiments of this paper. The z model (Pacanowski 1995) is based on a horizontal arrangement of variables in which both components of velocity are defined at the corners of a square of checkerboard pattern and temperature and pressure are defined in the center of the square (Arakawa B-grid). On the other hand, the layered model of Hallberg (Hallberg and Rhines 1996) defines the normal components of velocity in the center of each side of the checkerboard square (Arakawa C-grid). As pointed out earlier, the two models are configured to be similar by suppressing horizontal diffusion in the z model using the flux-corrected transport scheme.

A linearized equation of state depending only on temperature

TABLE 1. Summary of runs: "F" means a run with the flat-bottom basin, which is a standard case, "B" means one with the bowl-shaped basin, and "L" means one with 10 times longer restoring timescale ($\tau_T = 300$ days) than the standard case. In the layered model column, numbers in the parentheses represent the number of layers used.

κ (10^{-4} m^2 s^{-1})	z model	Layered model
0.05	F, W	F(17)
0.1	F, B, W	F(17), B(14)
0.2	F, B, L	F(11)
0.5	F	—
1	F, B, W, L	F(10), B(10)
2	F	F(8)
10	F, B, W	F(11), B(11)

$$\rho(T) = \rho_o[1 - \alpha(T - T_o)]$$

has been used in both models, where the thermal expansion coefficient α is 2×10^{-4} °C^{-1}. Therefore, buoyancy and temperature will be used interchangeably in the discussion of the experiments. Laplacian horizontal viscosity with the coefficient $A_h = 2.0 \times 10^5$ m^4 s^{-1} is used in both models. A no-slip boundary condition on velocity is used along all boundaries, except at the equator where an equatorial symmetry condition is imposed. Vertical viscosity is fixed at 1.0×10^{-2} m^2 s^{-1}.

Density gradients are imposed at the surface by damping the temperature through a layer of fixed depth h_s toward a reference temperature T_{air}, the familiar "Newtonian damping" condition (Haney 1974). The surface heat flux, therefore, is

$$q_T = \rho C_p \frac{h_s}{\tau_T}(T_{air} - SST). \qquad (8)$$

Here C_p is the specific heat of water, T_{air} varies linearly from 24°C at the equator to 0°C at the poleward boundary, and SST is the average temperature over h_s, which is taken to be 25 m. In the z model SST is taken to be the temperature of the first level. In the layered model SST is taken to be the average temperature of the upper 25 m, which may be occupied by one or more layers. For most of our experiments the damping timescale is taken to be 30 days, except for two runs in which $\tau_T = 300$ days. The longer timescale allows the upper-ocean temperature greater freedom to adjust itself as determined by the ocean circulation. This upper boundary condition was chosen to conform to that of earlier studies. However, in the analysis of the experiment it becomes clear that the condition violates the assumption of similarity if buoyancy forcing at the surface is treated the same as the meridional contrast of T_{air}. We will return to this point later.

A summary of the numerical experiments with the two models is given in Table 1. Experiments were carried out for both the cases of uniform depth and a bowl-shaped topography. In order to resolve the thermocline for the layered model cases in which very low vertical thermal diffusivity was used, more layers are adopted. The smaller number of experiments with the effect of
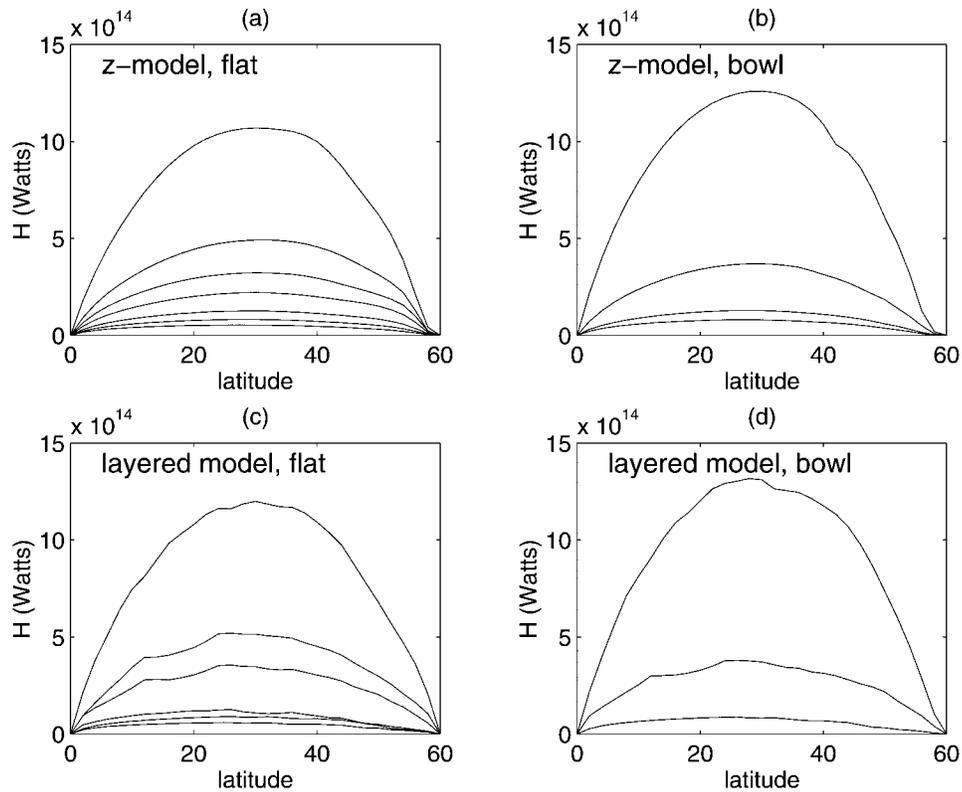
Fig. 2. Zonally averaged meridional heat transport profiles for different κ from the z model (a) with the flat bottom, (b) with the bowl-shaped bottom, and the layered model (c) with the flat bottom, and (d) with the bowl-shaped bottom. The vertical diffusivity of the profiles are (a) 10, 2, 1, 0.5, 0.2, 0.1, 0.05; (b) 10, 1, 0.2, 0.1; (c) 10, 2, 1, 0.2, 0.1, 0.05; and (d) 10, 1, 0.1 from top to bottom in 10^{-4} m^2 s^{-1}.

wind driving added, which are indicated by "W" in the table, were only carried out for uniform depth in the z model.

The procedure for carrying out the integrations was to start all z model runs from a state of rest with warm water filling the basin. Wind stress was absent in all cases. The numerical integration was then carried out for a period of 2–3 to 10 000 years. For large κ, the circulation oscillates with respect to time, so we obtained a statistical equilibrium state by averaging the last 500 years or so of the integration. For small κ, the period of integration is smaller than the diffusive time-scale for the total depth d^2/κ, where $d = 4000$ m, but the period was longer than the diffusive timescale of the thermocline, itself. In any case, the deep temperature change is less than 0.01°C over 1000 years. In those cases with winds, surface wind stress was turned on when the circulation reached (near) equilibrium states and then the model was integrated for about 2000 to 3000 years more. In the case of the layered model the integration was extended until the mean thickness of the lowest layer changed less than 1 m over 100 years. The bottom layer occupies most of the basin, so the layered model does not resolve the density structure of the deep water as well as the z model. Consequently a shorter

time was required to reach an equilibrium state in the layered model.

4. Results

a. Meridional heat transport

The profiles of poleward heat transport, H, for different cases are shown in Fig. 2. The amplitude of H depends on the magnitude of the vertical diffusivity, but the shape of the profiles remains nearly the same, as expected for self-similar solutions. A comparison of panels a and c for the flat bottom geometry case and panels b and d for the bowl-shaped case shows that the z model and the layered model give very similar results for poleward heat transport. This result may seem obvious, but as will be shown in Part II of this paper, many of the details of the z model and the layered-model solutions are quite different.

In Fig. 2, the H profiles for the layered model are less smooth than those for the z model. This roughness is a numerical artifact due to the vertical resolution in the layered model. There is no representation of the mixed layer in the layered model, so the outcrops of the layers appear right at the surface. The surface heat
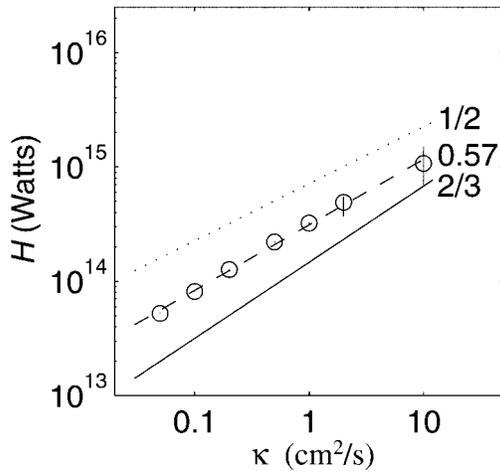
FIG. 3. Meridional heat transport at 30°N from the z model with the flat bottom vs the vertical diffusivity of heat κ. The slope of the solid line, the scaling law, is ⅔ and the slope of the dotted line is ½. The dashed line is the linear least squares fit, whose slope is 0.57 ± 0.04.
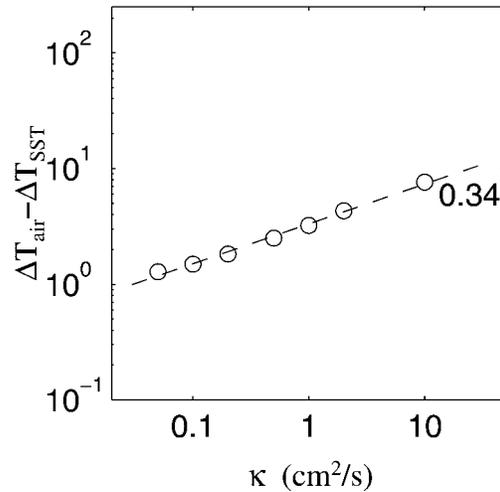
FIG. 4. Comparison of κ and the deviation of the meridional SST contrast from that of the reference temperature $\Delta T_{air} - \Delta T_{SST}$. Results from the z-model flat-bottom cases are used. The dashed line is the linear least squares fit, whose slope is 0.34.

flux, which depends on the difference between the surface temperature and a smoothly varying reference temperature, changes abruptly across the outcrops. This induces small-scale, shallow overturning cells anchored to the outcrops that alter the H profile locally. As the number of layers is increased, these overturning cells decrease in scale and the profile of H becomes smoother without significant changes in the overall shape.

Meridional heat transport H at 30°N from the flat-bottom z model case is shown as a function of κ in Fig. 3. The linear least squares fit to the results gives a slope of 0.57 ± 0.04. Note that this slope is quite similar to the results of previous studies based on z models as shown in Fig. 1. The slope falls about half-way between the ½ law favored by Colin de Verdière (1988) and Marotzke (1997) and the ⅔ law suggested by the scaling given in section 2.

In obtaining this result it is implicitly assumed that the meridional temperature contrast ΔT is uniformly proportional to the reference temperature imposed at the upper surface. In the experiment, this assumption was not satisfied. Since the Newtonian damping condition [Eq. (8)] yields not the temperature but heat flux, the sea surface temperature has some degrees of freedom to depart from the reference temperature depending on the strength of the circulation. Figure 4, in which κ and the deviation of the meridional SST contrast from that of the reference temperature $\Delta T_{air} - \Delta T_{SST}$ from the flat-bottom z model cases are compared, shows that the deviation scales quite well with $\kappa^{1/3}$ as does the velocity scale U. As κ becomes larger, the circulation intensifies and the water becomes less exposed to the air. The water in the polar (equatorial) region becomes less cold (warm) and the zonally averaged north–south sea surface temperature difference ΔT_{SST} decreases with in-

creasing κ. Therefore, if ΔT is considered as a fixed quantity, self-similarity on which the scaling law is based is violated. The ⅓ power dependence of $\Delta T_{air} - \Delta T_{SST}$ on κ as shown in Fig. 4 suggests that the Newtonian damping timescale τ_T in Eq. (8) should be proportional to the advective timescale $U/L \approx \kappa^{1/3}$ if we want to keep the buoyancy forcing fixed. The dependence of the coupling coefficient or $\Delta T_{air} - \Delta T_{SST}$ on the vertical diffusion has been ignored in previous studies.

Of course there are other ways in which the experiments are not strictly consistent. The scaling law and self-similarity also require an infinitely deep basin, but the total depth of the basin is kept constant in the numerical experiments. Thus the ratio of the scale depth to the total depth of the thermocline varies. However, as pointed out by Robinson and Stommel (1959) as long as this ratio is small, it should not matter, as the density gradient in the abyssal region below the thermocline is very small in any case. The most fundamental assumption involved in the scaling law is that the velocity is essentially geostrophic. Equivalently, the Rossby and Ekman numbers remain small throughout the range of the experiments. In the experiment the Ekman number $\nu/fd^2 \approx 2 \times 10^{-2} \ll 1$, where ν is the viscosity and d is the depth. The Rossby number $U/fL = g\alpha\Delta Td/f^2L^2 \approx 5 \times 10^{-2} \ll 1$. The basic assumption was satisfied. We conclude that inconsistencies involved in departures from geostrophy and the use of a fixed depth much larger than the depth of the thermocline are relatively unimportant, compared to the inconsistency of assuming a constant ratio between the imposed temperature difference and the realized temperature difference in the solutions.

Taking into account that the ratio of the sea surface temperature difference to the imposed temperature dif-
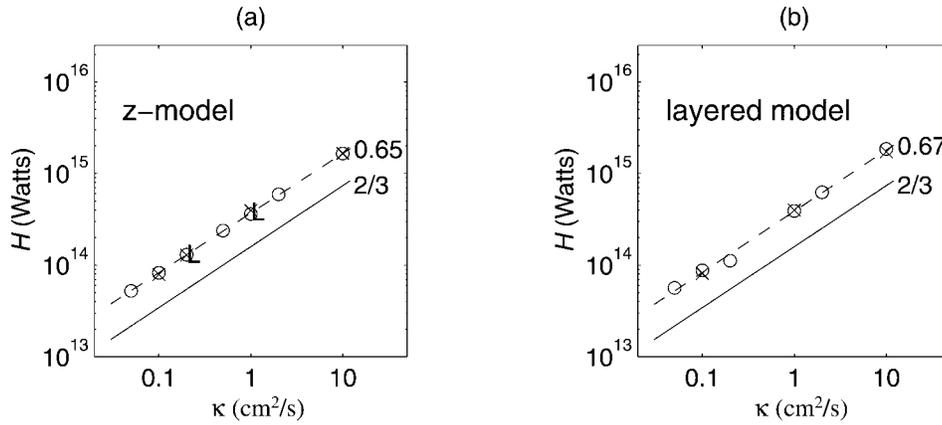
Fig. 5. Meridional heat transport at 30°N with SST correction vs κ (a) from the z-model runs and (b) from the layered-model runs. "○" is for a flat bottom case (F), "×" is for a bowl-shaped bottom case (B), and "L" is for a case with long τ_T. Solid lines represent the ⅔ scaling law. Dashed lines represent the linear least squares fit lines for the runs with the flat-bottom geometry in each case. The numbers represent the slopes of the fit lines.

ference is a function of κ, we rewrite Eqs. (4), (6), (7) by replacing ΔT with ΔT_{SST}, and moving it to the left-hand side, to obtain the following:

$$\delta_T(\Delta T_{\text{SST}}/\Delta T_{o,\text{SST}})^{1/3} \sim \kappa^{1/3},$$

$$\Psi(\Delta T_{\text{SST}}/\Delta T_{o,\text{SST}})^{-1/3} \sim \kappa^{2/3},$$

$$H(\Delta T_{\text{SST}}/\Delta T_{o,\text{SST}})^{-4/3} \sim \kappa^{2/3}. \qquad (9)$$

Here $\Delta T_{o,\text{SST}}$ is ΔT_{SST} with $\kappa = 0.05 \times 10^{-4}$ m² s⁻¹ and is used to normalize ΔT_{SST} so that the left-hand sides retain reasonable numerical values. The buoyancy at the sea surface is not determined by the restoring temperature but by SST, so ΔT_{SST} is the physically more relevant property.

In Fig. 5, the heat transport, H, at 30°N is plotted against κ with the temperature correction shown above [the left-hand side of Eq. (9c)]. In the layered model ΔT_{SST} is quantized by the layer configuration, and those data from the z model are used for the temperature correction. The results for the flat-bottom geometry and the bowl-shaped geometry nearly coincide for the corrected results, while they diverge as κ becomes larger for the original data. A shorter advection timescale relative to the fixed damping timescale means that the realized density difference is significantly less than the reference temperature difference for large κ. The same effect takes place when the restoring time is made longer in the experiments designated by "L." However, with the correction indicated above, the results for long and short restoring times become nearly indistinguishable as shown in Fig. 5.

The slopes of the least square fits for the corrected values of H are between 0.65 and 0.67 for all cases shown in Fig. 5 as predicted by the scaling on section 2. This provides an explanation of a large portion of the discrepancies shown in Fig. 1 between earlier results by Bryan (1987), Colin de Verdière (1988), and Mar-

otzke (1997) and the scaling law. As shown in Eq. (9), the dependences of Ψ and δ_T on the imposed density difference are smaller, so the effect of the correction is correspondingly less (about one-fourth of that for H). Hereafter comparisons with model results are made using the lhs of Eq. (9).

b. Strength of the overturning circulation

The traditional overturning transport streamfunction obtained from a zonal average along constant depth surfaces $\Psi(\theta, z)$ is

$$\Psi(\theta, z) \equiv \int_{\text{bottom}}^{z} \int_{E}^{W} v(\theta, z')\, dz'\, dx,$$

where θ is the latitude. Experimental results are shown in Fig. 6. For the flat-bottom case, as shown in other studies such as Winton (1997), the maximum transport streamfunction is very close to the poleward boundary. The downward branch of the meridional circulation is closely confined to the region near the northern wall. The experiments indicate that the maximum of Ψ has a power dependence on κ of 0.45 ± 0.04 as shown in Fig. 7. The result is different from the ⅔ power dependence predicted by the scaling given in section 2, but is comparable to what Huang and Chou (1994) found (Fig. 9 in their paper).

In the scaling of section 2, it is assumed that heat transport is simply proportional to δ_T times Ψ. In that case it makes more physical sense to define the overturning in isothermal, or equivalently for these simple models, isopycnal coordinates. In Fig. 8, the overturning streamfunction obtained by zonally integrating along isopycnals, $\Psi(\theta, \rho)$
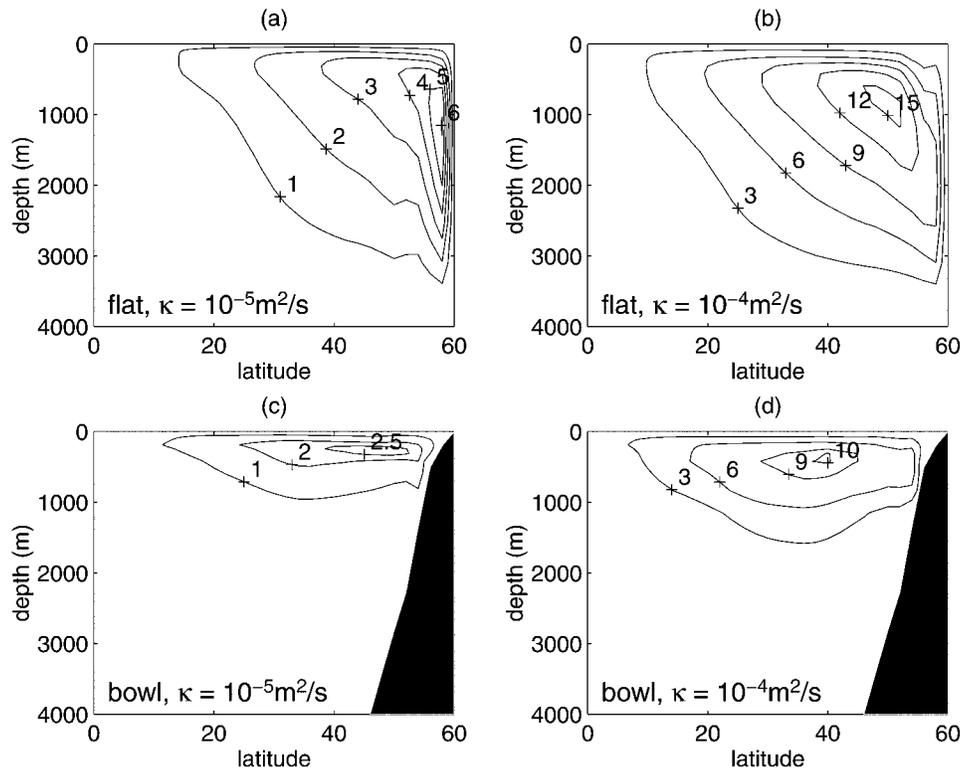
FIG. 6. Plot of $\Psi(z)$ from the z-model experiments with the flat-bottom geometry when (a) $\kappa = 0.1 \times 10^{-4}$ m^2 s^{-1}, (b) $\kappa = 1 \times 10^{-4}$ m^2 s^{-1}, and with the bowl-shaped bottom geometry when (c) $\kappa = 0.1 \times 10^{-4}$ m^2 s^{-1}, and (d) $\kappa = 1 \times 10^{-4}$ m^2 s^{-1}.

$$\Psi(\theta, \rho) \equiv \int_{E}^{W} \int_{\rho_{\text{bottom}}(x,\theta)}^{\rho} \frac{\partial z}{\partial \rho'} v(\theta, \rho') \, d\rho' \, dx$$

is shown.

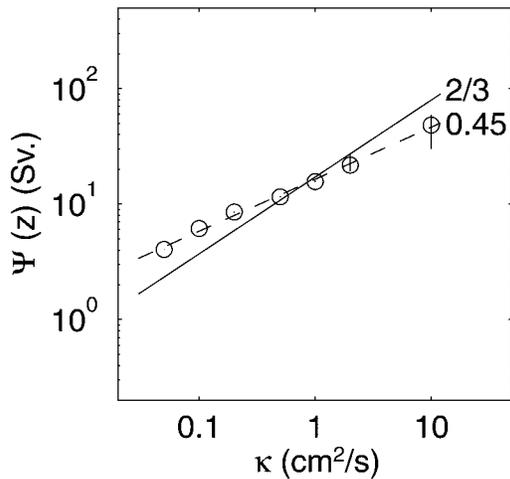For the flat-bottom case, the maximum of $\Psi(\rho)$ is significantly smaller than that of $\Psi(z)$. The difference

FIG. 7. The maximum of $\Psi(z)$ from the z-model flat bottom cases vs κ. Solid line represents the scaling law and dashed line is for the linear least-squares fit line, whose slope is 0.45 $\pm$ 0.04.

becomes relatively greater as κ decreases and the downward branch of the meridional circulation becomes more closely confined to the northern wall. The difference between $\Psi(\rho)$ and $\Psi(z)$ can be understood from Fig. 9, which shows results for the z model in a longitude by depth cross section near the northern wall for a low κ and medium κ cases. In a low κ case (Fig. 9b), there is a large amount of poleward flow at upper levels compensated by equatorward flow below 2000 m. This implies a large meridional transport defined along depth surfaces. On the other hand, the isopycnal surfaces are nearly vertical away from the eastern and western boundaries as shown in Fig. 9a. In a higher κ case, the meridional velocity section (Fig. 9d) also shows a large vertical shear as in the low κ case, but more than half of the area is stratified as the temperature section (Fig. 9c) shows. If the meridional flow is averaged on isopycnal surfaces, the low κ case shows relatively greater amount of cancellation between the poleward flow near the surface and the equatorward flow at the lower levels. This accounts for the much lower intensity of the meridional circulation shown in Fig. 8 ($\Psi(\rho)$) compared to that shown for depth surfaces in Fig. 6.

The bowl-shaped geometry cases also show temperature and velocity structures similar to Fig. 9 near the northern boundary. The volume of the northern region is small because of the bottom slope so that the circu-
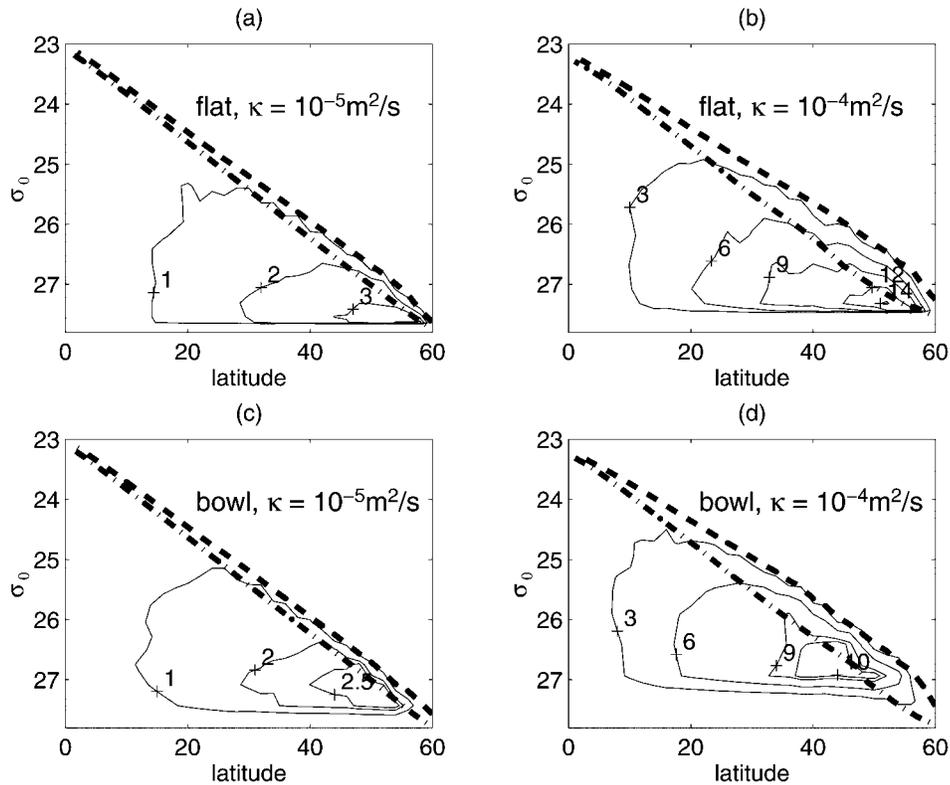
FIG. 8. Plot of $\Psi(\rho)$ from the z-model experiments with the flat-bottom geometry when (a) $\kappa = 0.1 \times 10^{-4}$ m^2 s^{-1}, (b) $\kappa = 1 \times 10^{-4}$ m^2 s^{-1} and with the bowl-shaped bottom geometry when (c) $\kappa = 0.1 \times 10^{-4}$ m^2 s^{-1}, (d) $\kappa = 1 \times 10^{-4}$ m^2 s^{-1}. Dash–dotted (dashed) lines represent the highest (lowest) surface density in each case.

lation along isotherms in the polar ocean does not make much contribution to $\Psi(z)$. Thus the difference between $\Psi(z)$ and $\Psi(\rho)$ is less pronounced for the bowl-shaped topography. Furthermore, Fig. 8 shows that $\Psi(\rho)$ maintains a robust similarity despite changes in κ as well as in geometry, while $\Psi(z)$ shown in Fig. 6 does not. In other words, $\Psi(\rho)$ shows weaker sensitivity to the geometry. This illustrates the effects of geometry and the importance of diagnosing the meridional circulation both in depth and isopycnal coordinates.

A comparison of Fig. 8 and Fig. 10, which shows $\Psi(\rho)$ from the layered models, allows an idea of the differences between the z model and the layered model. Qualitatively, the patterns for both models look very much alike. The most obvious difference is in the range of surface temperature. The lowest surface temperature at a latitude, a dashed line in the figures, is mostly determined by the air–sea heat exchange, so both models yield about the same results. The highest surface temperature, a dash–dotted line in the figures, is largely fixed by the advection of warm water from the south. The layered model solutions in Fig. 10 show a greater spread over all latitudes than the z-model solution in Fig. 8. This indicates that surface advection is more active in the layered model, especially along the eastern

boundary which results in important differences in the surface heating patterns. Those differences, which do not appear when zonal averaging is performed, will be explored in Part II.

The maxima of $\Psi(\rho)$ from the z model and the layered model versus κ are shown in Fig. 11. The slope of the least squares fit in each case is comparable with that predicted from the scaling law. In some previous studies, the meridional overturning from the maximum value in z coordinates was used, and major discrepancies with the scaling law were found. Winton (1997) found better agreement by using the meridional overturning in z coordinates, but instead of using the maximum value, he used the value well away from the poorly stratified region close to the poleward wall. Thus he avoided the problem illustrated by Fig. 9 and obtained much better agreement with the scaling in section 2.

At the midlatitudes where the meridional heat transport profiles are at their peaks, the z-model flat-bottom cases show $\Psi(z) \sim \kappa^{0.65}$ and $\Psi(\rho) \sim \kappa^{0.64}$, and the layered-model flat-bottom cases show $\Psi(\rho) \sim \kappa^{0.64}$. The slope of isotherms is small and the orientation of isotherms does not vary significantly with κ. The contribution of recirculation on isothermal surface to $\Psi(z)$ is small for all κ, so $\Psi(z)$ follows the scaling law well as
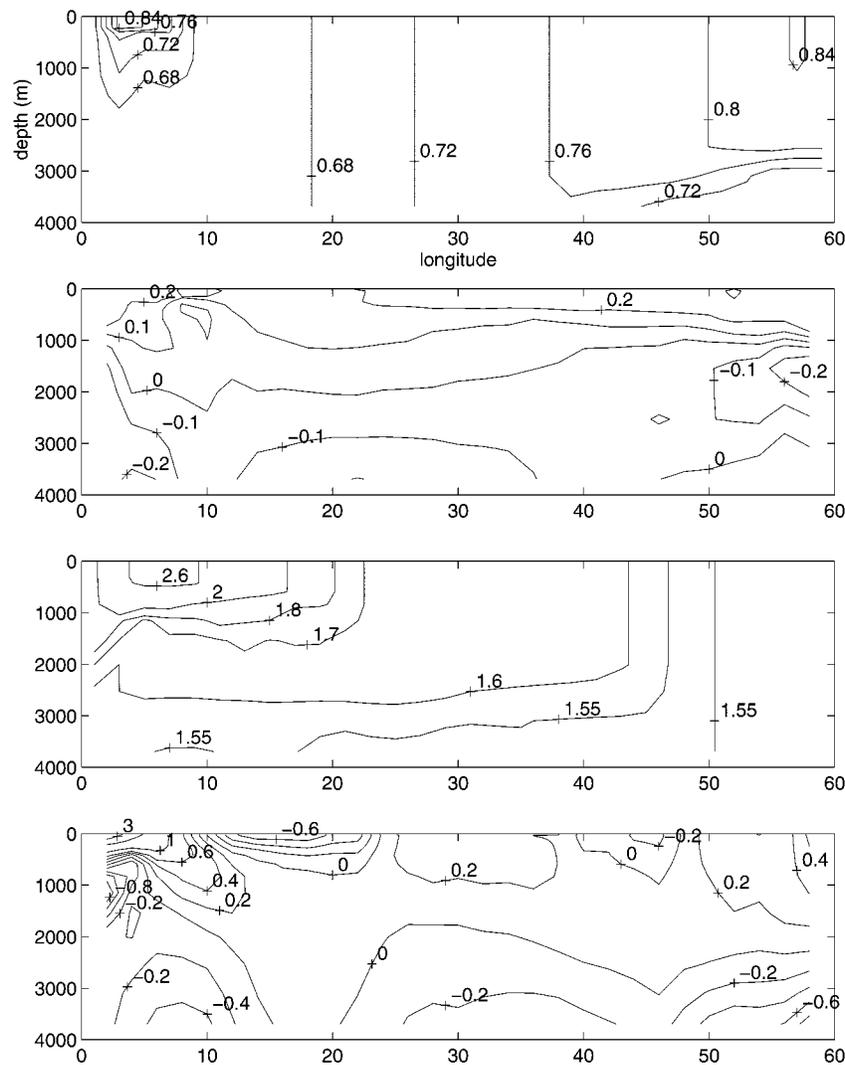
FIG. 9. The zonal sections of temperature [(a) and (c)], and the meridional velocity v in cm s^{-1} [(b) and (d)] along the northernmost grid points (59°N for T and 58°N for v) from the z-model flat-bottom cases. In (a) and (c) $\kappa = 0.1 \times 10^{-4}$ m^2 s^{-1} and in (c) and (d) $\kappa = 1 \times 10^{-4}$ m^2 s^{-1}.

$\Psi(\rho)$. In the layered model, layers outcrop and the vertical resolution becomes poorer to the north. In the z model, the number of levels does not decrease to the north, but the convective adjustment makes more water completely homogeneous and reduces the effective vertical resolution of tracer. Therefore, the circulation is resolved better in midlatitudes than in high latitudes. Furthermore, in midlatitudes nongeostrophic processes such as convective adjustment are weaker and the models are expected to follow the prediction from the scaling law better.

From the perspective of this study it is somewhat surprising that Marotzke (1997) found reasonable agreement between $\Psi(z)$ and the scaling law given in Eq. (6) even at high latitudes. However, there are a few factors that may explain the apparent discrepancy with the pre-

sent study. First, Marotzke's (1997) results are for a somewhat different model in which vertical diffusion is confined to a limited band along the meridional boundaries. Second, his area mean of κ varies from 0.54×10^{-4} to 3.6×10^{-4} m^2 s^{-1}, which is in the medium to high range of the present study. As shown in Figs. 9c and 9d vertical shear in the meridional velocity near the eastern boundary is the main factor that enhances $\Psi(z)$ relative to $\Psi(\rho)$ when κ is not small. According to Marotzke the effect of confining the vertical diffusion produces less vertical shear near the eastern boundary than the case with uniform vertical diffusion. Therefore in the boundary mixing case, the contribution of recirculation occurring along steep isothermal surfaces to $\Psi(z)$ is diminished so that $\Psi(z)$ follows the scaling law well.

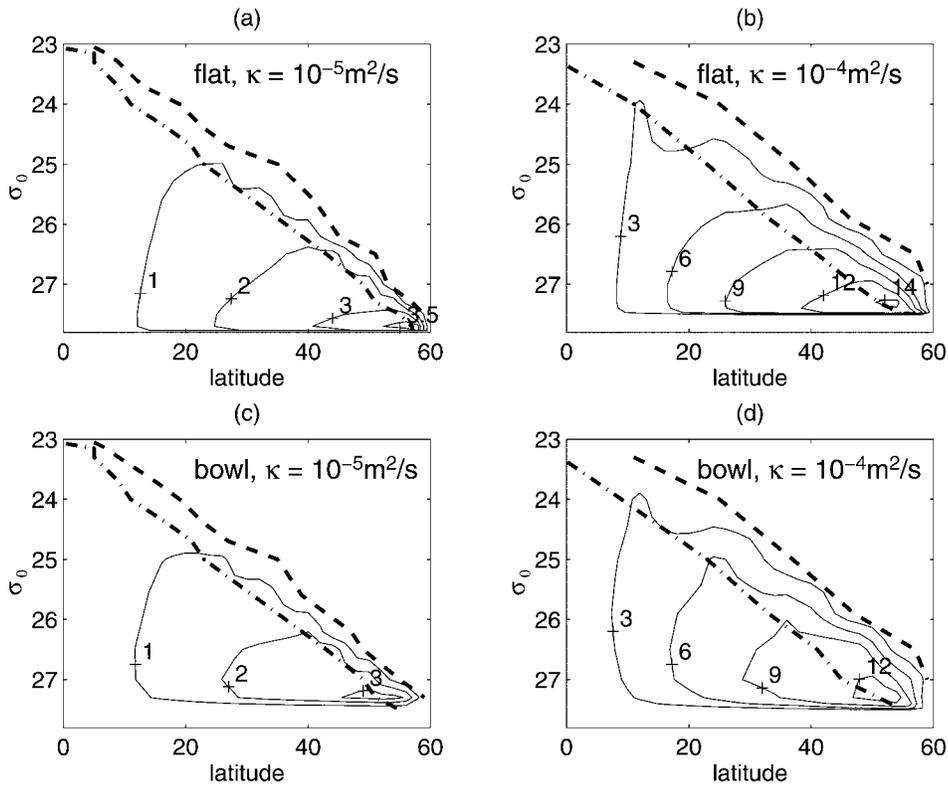Zhang et al. (1998) also found a good agreement be-

FIG. 10. Plot of $\Psi(\rho)$ from the layered model with the flat bottom geometry when (a) $\kappa = 0.1 \times 10^{-4}$ m^2 s^{-1}, (b) $\kappa = 1 \times 10^{-4}$ m^2 s^{-1}, and with the bowl-shaped bottom geometry when (c) $\kappa = 0.1 \times 10^{-4}$ m^2 s^{-1}, (d) $\kappa = 1 \times 10^{-4}$ m^2 s^{-1}. Dash–dotted (dashed) lines represent the highest (lowest) surface density in each case.

tween $\Psi(z)$ and the scaling law in their numerical experiment with eddy transport parameterization based on Gent and McWilliams (1990). The parameterization releases available potential energy by reducing the slope of steep isopycnals and the vertical shear, and thus suppresses the alignment problem. The difference between $\Psi(\rho)$ and $\Psi(z)$ becomes smaller so that $\Psi(z)$ also shows good agreement with the scaling law.
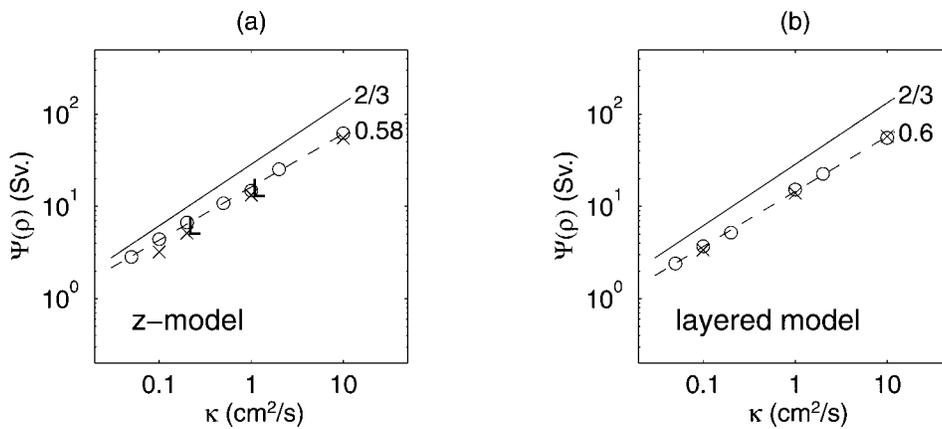

FIG. 11. The maximum of overturning circulation {max[$\Psi(\rho)$]} over the basin vs κ from the results of (a) the z model and (b) the layered model: "○" is for a flat bottom case (F), "×" is for a bowl-shaped bottom case (B), and "L" is for a case with long τ_T. Solid lines represent the ⅔ scaling law. Dashed lines represent the linear least squares fit lines for the runs with the flat bottom geometry in each case. The numbers represent the slopes of the fit lines.
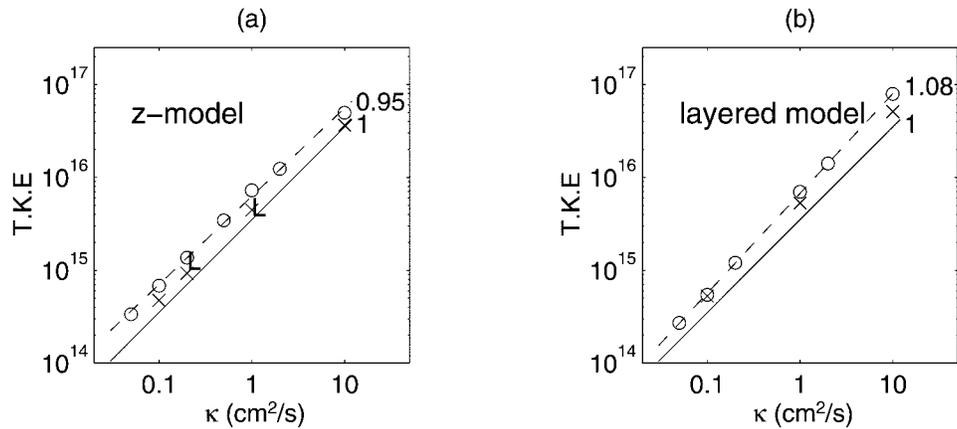
(a)

(b)

FIG. 12. Total kinetic energy vs κ from (a) the z-model results, and (b) the layered-model results: "○" is for a flat bottom case (F), "×" is for a bowl-shaped bottom case (B), and "L" is for a case with long τ_T. Solid lines represent the 1 power relation scaling law. Dashed lines represent the linear least squares fit lines for the runs with the flat bottom geometry in each case. The numbers represent the slopes of the fit lines.

The global kinetic energy of the model does not depend on the choice of a coordinate system, so it may be a more objective indicator of circulation intensity. Since the only length scale involved is the depth of the thermocline, the total kinetic energy, TKE, is

$$\text{TKE} \sim \delta_T U^2.$$

Making use of Eqs. (4) and (5)

$$\text{TKE} \sim \Delta T^{1/3} \kappa^1. \tag{10}$$

Results for TKE are plotted in Fig. 12. Colin de Verdière (1988) suggests that TKE $\sim U^2$ so TKE$^{1/2} \sim U \sim \kappa^{2/3}$, but his results show that TKE$^{1/2} \sim \kappa^{1/2}$, consistent with the present result.

c. Thickness of thermocline

A measure of the thickness of the thermocline at a single point in the horizontal is defined as follows:

$$\delta_T(x, y) \equiv \frac{\int_{\text{bottom}}^{\text{top}} (T - T_{\text{bottom}})z \, dz}{\int_{\text{bottom}}^{\text{top}} (T - T_{\text{bottom}}) \, dz}. \tag{11}$$

In Fig. 13 the values of thermocline thickness, δ_T which are obtained from zonal averages at 30°N, excluding areas close to the lateral boundaries, are shown as a function of κ. As shown in previous studies the exper-
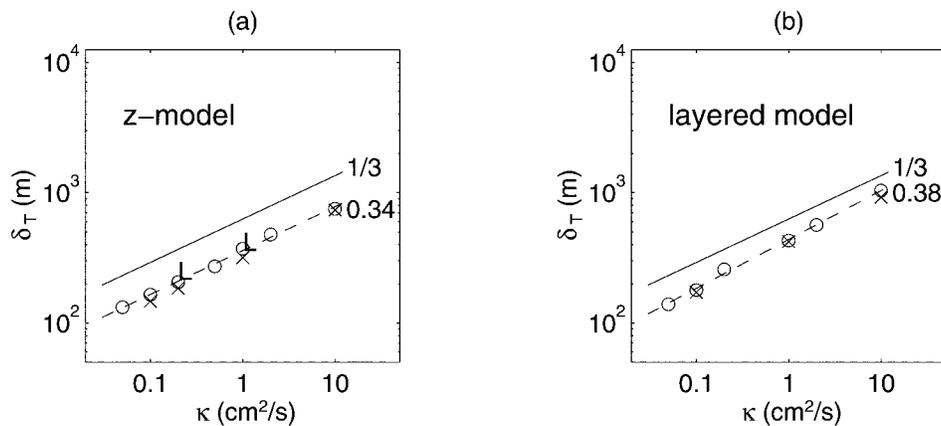
(a)

(b)

FIG. 13. The thickness of thermocline (δ_T) from (a) the z-model results, and (b) the layered model results: "○" is for a flat bottom case (F), "×" is for a bowl-shaped bottom case (B), and "L" is for a case with long τ_T. Solid lines represent the ⅓ power relation scaling law. Dashed lines represent the linear least squares fit lines for the runs with the flat bottom geometry in each case. The numbers represent the slopes of the fit lines.

imental results are in reasonable agreement with the scaling of section 2. Equation (11) is rather sensitive to the details of the deep-water density structure, which is resolved in more detail in the z model than in the layered model in our experiments. Thus for this particular choice of depth levels in the z model and choice of layers in the layered model, the z model is more accurate for estimating the thermocline depth.

d. Comparison of the zonal and meridional pressure gradients

One of the assumptions made during the derivation of the scaling law is that the horizontal patterns of the solutions are self-similar and only the depth scale of the thermocline changes with the magnitude of the vertical diffusivity. This means that the zonal and meridional pressure gradients will be proportional, so that a scale velocity based on the meridional pressure gradient will be a good measure of the meridional velocity. The relationship of meridional pressure gradient and zonal pressure gradient or meridional mass transport has been investigated in previous studies by Wright and Stocker (1991) and Hughes and Weaver (1994), but these studies only considered a limited range of parameters and did not show self-similarity. Here, we compare the zonal and meridional pressure gradients using results from the z model flat bottom cases in which $0.05 \times 10^{-4} < \kappa < 10 \times 10^{-4}$ m s^{-1}.

The hydrostatic equation $p_z = -\rho z$ can be integrated from the surface to some depth to yield

$$p(x, y, z) = p_s(x, y) + g \int_z^0 \rho(x, y, z') \, dz'$$

$$= p_s(x, y) + p_{bc}(x, y, z),$$

where p_s is the surface pressure, which is the sum of the atmospheric pressure and the pressure that would be exerted by a rigid lid placed on the top of the ocean. Since p_s is independent of z, the mean zonal and meridional gradients of baroclinic pressure p_{bc} yields scales of the baroclinic component of meridional and zonal velocities, respectively. An expression for the mean zonal baroclinic pressure gradient is

$$\frac{\Delta p_{bc}(z)}{\Delta X(y)} = -\rho_o g \alpha \Delta X(y)^{-1}$$

$$\times \left(\int_z^0 T(X_E, y, z') - \int_z^0 T(X_W, y, z') \right) dz'.$$

Here, X_W and X_E are the locations of the western and the eastern boundaries and $\Delta X(y) = X_E - X_W$. We can define the zonal average of mean meridional baroclinic pressure gradient

TABLE 2. Ratio of the vertical mean of the zonally averaged zonal pressure gradient to that of the meridional pressure gradient over the thermocline r_m at 30°N.

	κ (10^{-4} m^2 s^{-1})						
	0.05	0.1	0.2	0.5	1	2	10
r_m	−0.15	−0.15	−0.15	−0.16	−0.17	−0.17	−0.15

$$\frac{\Delta p_{bc}(z)}{\Delta Y} = -\rho_o g \alpha \Delta Y^{-1}$$

$$\times \overline{\left(\int_z^0 T(Y_N, x, z') \, dz' - \int_z^0 T(Y_S, x, z') \, dz \right)}.$$

Here, the overbar represents a zonal average, Y_S and Y_N are the locations of the southern and the northern boundaries, and $\Delta Y = Y_N - Y_S$.

The scaling law described in section 2 predicts global properties, so properly averaged quantities would be better measures for the scaling law than quantities at certain location. A measure of the mean zonal density gradient for the thermocline can be obtained from the the vertical mean of the mean zonal density gradient over the thermocline, that is, $[\Delta p_{bc}(\delta_T(\kappa))/\Delta X]/\delta_T(\kappa)$. Similarly, a measure of the mean meridional density gradient can be obtained from $\Delta p_{bc}(\delta_T)/\Delta Y$. At 30°N the results from the flat-bottom z-model cases show that the ratio of $[\Delta p_{bc}(\delta_T(\kappa))/\Delta X]/\delta_T(\kappa)$ to $[\Delta p_{bc}(\delta_T)/\Delta Y]/\delta_T$ is between −0.27 and −0.26, while κ varies from 0.05×10^{-4} to 10×10^{-4} m^2 s^{-1}. Therefore, we can use a measure of the mean meridional density gradient for a measure of the mean zonal density gradient.

Since the mean horizontal pressure gradients at a certain level represent the scale of baroclinic velocities only at that level, we obtain measures of the mean meridional and zonal baroclinic velocities appropriate for the thermocline from the vertical means of $\Delta p_{bc}/\Delta X$ and $\Delta p_{bc}/\Delta Y$ over the thermocline; that is,

$$\left\langle \frac{\Delta p_{bc}}{\Delta X(y)} \right\rangle = \frac{1}{\delta_T(\kappa)} \int_{z=-\delta_T(\kappa)}^0 \frac{\Delta p_{bc}(z')}{\Delta X(y)} \, dz' \quad \text{and}$$

$$\left\langle \frac{\Delta p_{bc}}{\Delta Y} \right\rangle = \frac{1}{\delta_T(\kappa)} \int_{z=-\delta_T(\kappa)}^0 \frac{\Delta p_{bc}(z')}{\Delta Y} \, dz',$$

respectively. The ratio of $\langle \Delta p_{bc}/\Delta X \rangle$ to $\langle \Delta p_{bc}/\Delta Y \rangle$, r_m

$$r_m = \frac{\langle \Delta p_{bc}/\Delta X \rangle}{\langle \Delta p_{bc}/\Delta Y \rangle}$$

represents the ratio of the baroclinic meridional velocity scale to the baroclinic zonal velocity scale.

In Table 2, r_m from the z-model flat-bottom cases and δ_T estimated using Eq. (11) at 30°N, where the meridional heat transport becomes maximum, is shown. As we see in the table, over the entire range of κ in the experiments the ratio r_m is between −0.15 and −0.17 in spite of the fact that the scale depth of the thermocline
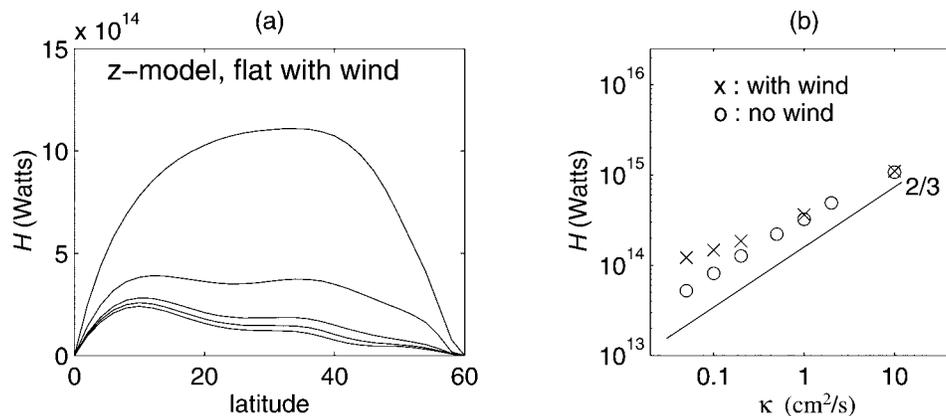
FIG. 14. Results from the *z* model with surface wind stress (a) meridional heat transport profiles and (b) meridional heat transport at 30°N (×) vs κ. In (b) the results from flat bottom cases (○) are also shown for comparison. The SST correction is not applied in this figure. Solid line in (b) represents the ⅔ scaling law.

varies by almost a factor of 6 ($\approx 200^{1/3}$) as shown in Fig. 13. This result provides additional confirmation that the solution have similar horizontal structure and justifies a posteriori the use of the zonal velocity scale to measure the meridional velocity scale in section 2.

e. The effect of wind stress

Our experiments would not be complete without some consideration of the effect of wind, which plays such an important role in determining the configuration of the thermocline and poleward heat transport in the real oceans. To illustrate the effects of wind, a zonally uniform wind stress based on the analytic expression of Bryan (1987) is used. The wind-driven gyre brings warm water to the north and cold water to the south, so the gyre enhances poleward heat transport. This is shown by a comparison of Fig. 14a and Fig. 2a. It is obvious from Fig. 14a that including wind does not allow self-similarity in the profiles of heat transport. In the Tropics, the Ekman transport causes the upwelling of the cold deep water to the surface so the air–sea heat exchange intensifies. So does the poleward heat transport. In midlatitudes, the Ekman transport induces downwelling of the surface water so that the air–sea heat exchange weakens. The poleward heat transport shows a local minimum. As κ increases, the interior vertical velocity due to the convergence and the divergence of the Ekman transport becomes relatively weaker than that due to the thermal forcing. For large κ, the thermohaline effects dominate so that the profile of poleward heat transport is nearly symmetric about 30°N. As κ decreases the contribution of the Ekman transport becomes dominant and an asymmetry about 30°N becomes more and more pronounced.

The dependence of *H* at 30°N on κ is shown in Fig. 14(b) by "×"s. The equivalent experiments without wind are shown by circles. Note that the poleward heat transport values coincide for large values of κ since the

thermohaline circulation dominates for those cases. As κ becomes smaller, the wind-driven transport plays an increasingly important role and there is a larger and larger departure from the scaling law given in section 2. This helps to explain the results of Hu (1996) shown in Fig. 1, since in his experiment with an isopycnal model the thermal forcing is relatively weak, and the effects of wind are included. Thus it seems likely that effects of wind may dominate for all of his heat transport results shown in Fig. 1.

5. Summary and conclusions

There is an urgent need to compare numerical models of the ocean circulation with different numerical architectures. This study is aimed to complement studies like the DYNAMO Project, in which the comparison of different architectures is based on complex models of the circulation in realistic geometrical settings. We have chosen to carry out experiments with two well-known types of models in very idealized geometries with simplified thermal forcing fields. While the simplicity of the experimental configuration does not allow direct comparison with observations, the experiments have the advantage of being much easier to analyze, and allowing much more insight into the basic processes involved. In addition it is possible to study model solutions that are in equilibrium with surface boundary conditions. This is very important for predicting how useful an ocean circulation model will be as one component of a coupled ocean–atmosphere climate model.

As a basis for the model comparison we have chosen a very simple paradigm of the ocean circulation, a buoyancy-driven circulation in which wind driving is absent. For realistic regimes in which the Rossby number and horizontal Ekman number are small, thermocline theory indicates that the vertical diffusion is the only significant parameter. The patterns of circulation should be horizontally self-similar with only a change in the intensity

of the circulation and the vertical scale (Robinson and Stommel 1959; Bryan and Cox 1967). In addition to testing the models, one of the objectives of this study was to determine why some previous numerical studies have not found very good agreement with thermocline scaling.

Experiments were carried out in which the vertical diffusivity, κ, was varied over a range of 200 with the two model architectures. In cases of uniform depth, the layered and the z-level models were found to yield nearly the same poleward heat transports in response to zonally uniform thermal forcing at the surface. Difficulties in the interpretation of earlier experiments are traced to the use of the Newtonian damping condition at the surface with fixed mixed layer depth and damping timescale. This violates similarity if the buoyancy forcing at the surface is considered fixed since the damping timescale is a function of κ. The results only agree with traditional scaling if the "realized" temperature gradients in the experiments rather than the gradients from the reference temperature are used as input to scale the results. The maximum of meridional overturning circulation in our experiment shows good agreement with the scaling law in both models if the meridional overturning streamfunction is estimated along isothermal surfaces instead of along level surfaces. This is due to the existence of extra circulations in the meridional plane, which are uncoupled to the thermohaline circulation and amplify the overturning in the meridional plane along level surfaces. This effect is particularly strong near the poleward boundary and for weak vertical diffusion. Two recent studies, Marotzke (1997) and Zhang et al. (1998), present results that appear to be inconsistent with this conclusion. In our analysis we identify the special factors in each of these studies that allowed a fit of the meridional overturning in level coordinates to scale theory, which we could only find for overturning in density coordinates. Horizontal self-similarity is tested by calculating the ratio of the vertical mean of the zonally averaged zonal pressure gradient to the vertical mean of the zonally averaged meridional pressure gradient over the thermocline. For solutions in which the thermocline depth varies by nearly a factor of 6, this ratio is constant within a few percent.

The agreement between the two model architectures in poleward heat transport is encouraging from the standpoint of ocean climate modeling since a major role of the ocean is to transfer heat poleward. However, details of climate are sensitive to the horizontal patterns of heat exchange between the ocean and atmosphere. In this respect the models show very significant differences. These differences appear to be associated with the way in which advection and convection are treated in the isopycnal and the z-level models. An analysis will be given in Part II.

Although we did not estimate the effects of numerical dispersion errors in the z model directly, a comparison of the z-model results with the layered model results shows that these errors do not seriously interfere with the interpretation of the z-model experiments. As shown in Fig. 5, 11, 12, and 13, the z-model results are about the same as those of the layered model that is not susceptible to the Veronis effect. The figures also show the z-model results do not show any noticeable change in the tendency to the lowest κ considered. If there were numerical diapycnal mixing, its magnitude would be significantly smaller than that for explicit diapycnal mixing. As shown in Fig. 3 and 7, our scaling results are comparable to those of earlier studies if we use $\Psi(z)$ and do not consider the effect of SST as in those studies. This suggests that the horizontal and vertical advection errors may not cause serious numerical mixing in those studies for the range of κ considered.

To test the robustness of the results to bottom topography, parallel experiments with both types of models were carried out in a bowl-shaped geometry. The geometry changed many aspects of the horizontal circulation especially in the z-level model, but the global or zonally averaged properties of interest to climate such as meridional heat and mass transports are comparable to those of the flat-bottom cases. The same scaling law applies to both models for the bowl-shaped geometry as it does for the uniform depth cases.

The close comparison of the scaling law and globally or zonally averaged properties of the solutions, irrespective of their differences explained in Part II of this paper, suggests that geostrophy and advective–diffusive heat balance constrain the overall properties of the thermohaline circulation of the model ocean.

REFERENCES

Boris, J. P., and D. L. Book, 1973: Flux-corrected transport. I. SHAS-TA: A fluid transport algorithm that works. *J. Comput. Phys.,* **11,** 38–69.

Bryan, F., 1987: Parameter sensitivity of primitive equation ocean general circulation models. *J. Phys. Oceanogr.,* **17,** 970–985.

Bryan, K., and M. D. Cox, 1967: A numerical investigation of the oceanic general circulation. *Tellus,* **19,** 54–80.

Colin de Verdière, A., 1988: Buoyancy driven planetary flows. *J. Mar. Res.,* **46,** 215–265.

DYNAMO Group, 1997: DYNAMO: Dynamics of North Atlantic models: Simulation and assimilation with high-resolution models. Report 294, Institut für Meereskunde, Kiel, Germany, 334 pp.

Gent, P. R., and J. C. McWilliams, 1990: Isopycnal mixing in ocean circulation models. *J. Phys. Oceanogr.,* **20,** 150–155.

Hallberg, R., and P. Rhines, 1996: Buoyancy-driven circulation in an ocean basin with isopycnals intersecting the sloping boundary. *J. Phys. Oceanogr.,* **26,** 913–940.

Haney, R. L., 1974: A numerical study of the response of an idealized ocean to large-scale surface heat and momentum flux. *J. Phys. Oceanogr.,* **4,** 145–167.

Hu, D., 1996: On the sensitivity of thermocline depth and meridional heat transport to vertical diffusivity in OGCMs. *J. Phys. Oceanogr.,* **26,** 1480–1494.

Huang, R. X., and R. L. Chou, 1994: Parameter sensitivity study of saline circulation. *Climate Dyn.,* **9,** 391–409.

Hughes, T. M. C., and A. J. Weaver, 1994: Multiple equilibria of an asymmetric two-basin ocean model. *J. Phys. Oceanogr.,* **24,** 619–637.

Ledwell, J. R., A. J. Watson, and C. S. Law, 1993: Evidence for slow mixing across the pycnocline from an open-ocean tracer-release experiment. *Nature,* **364,** 701–703.

Lineikin, P. S., 1955: On the determination of the thickness of the baroclinic layer in the sea. *Dokl. Akad. Nauk USSR,* **101,** 461–464.

Marotzke, J., 1997: Boundary mixing and the dynamics of three-dimensional thermohaline circulations. *J. Phys. Oceanogr.,* **27,** 1713–1728.

Munk, W. H., 1966: Abyssal recipes. *Deep-Sea Res.,* **13,** 707–730.

Pacanowski, R. C. P., 1995: MOM2 documentation. User's guide and reference manual. GFDL Ocean Tech. Rep. No. 3, 232 pp. [Available from Geophysical Fluid Dynamics Laboratory/NOAA, P.O. Box 308, Princeton, NJ 08542.]

Robinson, A., and H. Stommel, 1959: The oceanic thermocline and the associated thermohaline circulation. *Tellus,* **3,** 295–308.

Veronis, G., 1975: The role of models in tracer studies. *Numerical Models of Ocean Circulation,* Natl. Acad. Sci., 133–146.

Welander, P., 1986: Thermocline effects in the ocean circulation and related simple model. *Large-Scale Transport Processes in Oceans and Atmosphere,* J. Willebrand and D. L. T. Anderson, Eds., D. Reidel, 163–200.

Winton, M., 1996: The role of horizontal boundaries in parameter sensitivity and decadal-scale variability of coarse-resolution ocean general circulation models. *J. Phys. Oceanogr.,* **26,** 289–304.

——, 1997: The damping effect of bottom topography on internal decadal-scale oscillations of the thermohaline circulation. *J. Phys. Oceanogr.,* **27,** 203–208.

Wright, D. G., and T. F. Stocker, 1991: A zonally averaged ocean model for the thermohaline circulation. Part I: Model development and flow dynamics. *J. Phys. Oceanogr.,* **21,** 1713–1724.

Zhang, J., R. Schmitt, and R. X. Huang, 1999: The relative influence of diapycnal mixing and hydrologic forcing on the stability of the thermohaline circulation. *J. Phys. Oceanogr.,* **29,** 1096–1108.